JCB Article

KIFC3, a microtubule minus end–directed motor for the apical transport of annexin XIIIb–associated Triton-insoluble membranes

Yasuko Noda, Yasushi Okada, Nobuhito Saito, Mitsutoshi Setou, Ying Xu, Zheizeng Zhang, and Nobutaka Hirokawa

Department of Cell Biology and Anatomy, Graduate School of Medicine, University of Tokyo, Hongo, Tokyo 113-0033, Japan

We have identified and characterized a COOH-terminal motor domain–type kinesin superfamily protein (KIFC), KIFC3, in the kidney. KIFC3 is a minus end–directed microtubule motor protein, therefore it accumulates in regions where minus ends of microtubules assemble. In polarized epithelial cells, KIFC3 is localized on membrane organelles immediately beneath the apical plasma membrane of renal tubular epithelial cells in vivo and polarized MDCK II cells in vitro. Flotation assay, coupled with detergent extraction, demonstrated that KIFC3 is associated with Triton X-100–insoluble membrane organelles, and that it overlaps with apically transported TGN-derived vesicles. This was confirmed by immunoprecipitation and by GST pulldown experiments showing the specific colocalization of KIFC3 and annexin XIIIb, a previously characterized membrane protein for apically transported vesicles (Lafont, F., S. Lecat, P. Verkade, and K. Simons. 1998. *J. Cell Biol.* 142:1413–1427). Furthermore, we proved that the apical transport of both influenza hemagglutinin and annexin XIIIb was partially inhibited or accelerated by overexpression of motor-domainless (dominant negative) or full-length KIFC3, respectively. Absence of cytoplasmic dynein on these annexin XIIIb–associated vesicles and distinct distribution of the two motors on the EM level verified the existence of KIFC3-driven transport in epithelial cells.

Introduction

In polarized epithelial cells, the plasma membrane (PM)* is separated into apical and basolateral domains by tight junctions, and each domain has a distinct population of functional molecules and membrane composition. To maintain these compartments, differential transport is essential. Previous studies have revealed that this mechanism is carried out by four regulation processes (Grindstaff et al., 1998): packaging, transport, docking, and retention and/or removal. At the level of ER–Golgi–TGN, specific signals of a molecule at the cytoplasmic region are required for segregation into basolaterally transported membranes (Hunziker et al., 1991). For the apically transported membranes, a higher affinity to cholesterol-rich micromembrane domains, called rafts, or detergent-insoluble glycolipid-enriched domains, is proposed to be determinative for this cargo packaging (Harder and Simons, 1997). Thus, membrane proteins, either apically or basolaterally targeted, are packaged into their specific transport vesicles. These vesicles are transported to their specific destinations along microtubules (MTs) and/or actin networks or by simple diffusion. At the PM, a specific docking mechanism mediated by the specific t- and v-SNARE complex pairing guarantees the fusion of the transported vesicles to the proper PM subregion (Calakos et al., 1994; Rothman and Warren, 1994). Selective retention and/or removal of the PM protein during endocytosis–exocytosis cycling will proofread the missorting. Furthermore, the endocytosed missorted proteins may be transported to their proper destination through the transcytosis pathway (Matter and Mellman, 1994).

Among the aforementioned processes, the packaging, docking, and retention mechanisms have been vigorously examined. An increasing number of cytoplasmic determinants for basolateral targeting have been identified, and removal or inactivation of these signals is shown to cause aberrant

Address correspondence to Nobutaka Hirokawa, Department of Cell Biology and Anatomy, Graduate School of Medicine, University of Tokyo, Hongo, Tokyo 113-0033, Japan. Tel.: 81-3-5841-3326. Fax: 81-3-5802-8646. E-mail: hirokawa@m.u-tokyo.ac.jp

*Abbreviations used in this paper: aa, amino acid; AMP-PNP, adenylyl imidodiphosphate; BFA, Brefeldin A; DIC, dynein intermediate chain; gp, glycoprotein; GST, glutathione *S*-transferase; HA, haemagglutinin; KIF, kinesin superfamily protein; mβCD, methyl-β-cyclodextrin; MT, microtubule; PM, plasma membrane.

Key words: kinesin; kinesin superfamily proteins; apical transport; cholesterol; annexin XIIIb

destination of the molecules, reflecting their missorting and/or improper retention. Concurrently, t-SNAREs that are differentially distributed on the PM subdomain and their specific partner v-SNAREs have been identified. Moreover, the membrane-specific docking mechanism is now being elucidated at the molecular level (Yeaman et al., 1999). Clarification of the retention mechanism has also led to the identification of the endosomal localization signal and structural markers (Aroeti and Mostov, 1994; Mellman, 1996).

On the contrary, very little is known about the transport process. It is yet unclear whether a selective transport system exists for either apical or basolateral targeting. MT motors are expected to carry transport vesicles along the MT network. In fact, disruption of the MT network by nocodazole treatment significantly, though not completely, inhibits the delivery of newly synthesized membrane proteins to the PM. Furthermore, such treatment also causes missorting of some apical molecules to the basolateral membrane (Breitfeld et al., 1990; Grindstaff et al., 1998), suggesting the role of MT motors in the sorting process.

However, the degree of the transport machinery's contribution to the membrane sorting system is controversial at present (Salas et al., 1986; Drubin and Nelson, 1996), as there are several problems related to the detection system used. First, previous studies have evaluated the efficiency and accuracy of membrane sorting by measuring the final amount of targeted molecules in each PM subregion. This classical method has successfully identified many targeting signals of each membrane protein because it can sensitively and quantitatively assay the efficiency and accuracy of the entire membrane sorting system. However, this method is not sensitive enough to dissect each possible subprocesses, as it only monitors the final result: the amount of protein on the PM. For example, if the docking and retention mechanisms remain intact, the effect of missorting preceding these processes will be underscored (Grindstaff et al., 1998). As a result, this method is not sensitive for evaluating the contribution of the putative selective transport step.

To overcome this limitation, a direct evaluation of the membrane transport within a cell is important. Recent progress in quantitative confocal microscopy has enabled monitoring of the dynamic movement of fluorescence-tagged molecules in living cells (Lippincott-Schwartz et al., 1998; Nakata et al., 1998), and individual transported intermediate vesicles are visualized within the cells. This method has been successfully applied to quantitatively estimate the kinetics of membrane traffic in nonpolarized cells (Hirschberg et al., 1998). To estimate the real contribution of the putative selective transport system, possibly mediated by a specific MT motor in polarized cells, we adopted a method by which transport to the sub-PM region was evaluated based on the fluorescence intensity of the molecules in the sub-PM region by quantitative confocal microscopy. This method enables direct examination of the transport from the TGN to the apical PM.

The involvement of cytoplasmic dynein and kinesin superfamily proteins (KIFs) in apical transport has been reported (Lafont et al., 1994; Fath et al., 1997; Kraemer et al., 1999; Kreitzer et al., 2000); however, their role in selective transport is not yet established. Futhermore, research has not yet identified which KIF is involved in the apically targeted transport. In polarized epithelial cells, MTs usually display an apicobasal alignment with their minus ends oriented towards the apical region of the cells (Bacallao et al., 1989). Thus, the apically targeted transport should be conveyed by the MT minus end–directed motor whose directionality is opposite to that of most KIFs, including conventional kinesin. This suggests that some new minus end–directed KIFs may be involved in apically targeted transport.

Our recent systematic search for new KIFs (Nakagawa et al., 1997; Hirokawa, 1998a) demonstrated the existence of COOH-terminal motor domain–type KIFs (KIFCs) that are expected to be minus end–directed motors. KIFC3 is one of these new KIFCs and is abundant in the kidney, thus, it is a good candidate for the apically targeted transport motor in epithelial cells.

In this study, we cloned the full-length cDNA of KIFC3 and showed its property as a minus end–directed motor. KIFC3 is associated with apically targeted transport vesicles conveying annexin XIIIb and haemagglutinin (HA). The overexpression of KIFC3 and its dominant-negative form demonstrated the function of KIFC3 in apically targeted transport. The absence of the dynein–dynactin complex on KIFC3-associated vesicles suggests the existence of at least two independent apically targeted transport pathways: KIFC3- and cytoplasmic dynein–dynactin-dependent transport.

Results

Cloning of KIFC3 with KIFC consensus sequences

We cloned KIFC3 with primers corresponding to KIFC consensus sequence, a well-conserved sequence among KIFCs (Fig. 1 A) (Saito et al., 1997). As expected, the open reading frame of the cloned cDNA of KIFC3 consists of 824 amino acids (aa) (Fig. 1 B) (GenBank/EMBL/DDBJ accession number D49546), with the motor domain (aa 444–824) at the COOH terminus. Secondary structure and coiled coil prediction revealed that the central part of the molecule forms an α-helical coiled coil stalk between the globular domains at the NH_2 and COOH termini (Fig. 1 C). Homology search of the GenBank database predicted that KIFC3, as previously reported (Nakagawa et al., 1997; Yang, 1997; Hoang et al., 1998), is the founding member of a new KIFC subfamily that includes a fish protein MsFKIF2 and a *Xenopus* protein XlCTK1 (Bost-Usinger et al., 1997; Hoang et al., 1998).

KIFC3 existed ubiquitously among tissues. Northern blot analysis (Fig. 1 D, arrow) as well as immunoblotting assay (Fig. 1 E) revealed the expression of the KIFC3 protein in most of the tissues examined and predominantly in the kidney.

As shown in Fig. 1, E and F, the antibody against the recombinant KIFC3 rod fragment recognized three or four bands of protein in the total homogenate of the kidney (asterisks); these multiple bands were not detected in KIFC3 knockout mice (Fig. 1 F, right lane) (unpublished data). Because only the highest band was recognized by the anti-KIFC3 NH_2 terminus antibody (unpublished data), the lower bands are NH_2-terminally truncated proteins that may be produced by posttranslational modification or specific degradation pathway, as no splice variants were detected by the cap site hunting reverse transcription–PCR (Fig. 1 G, arrow).

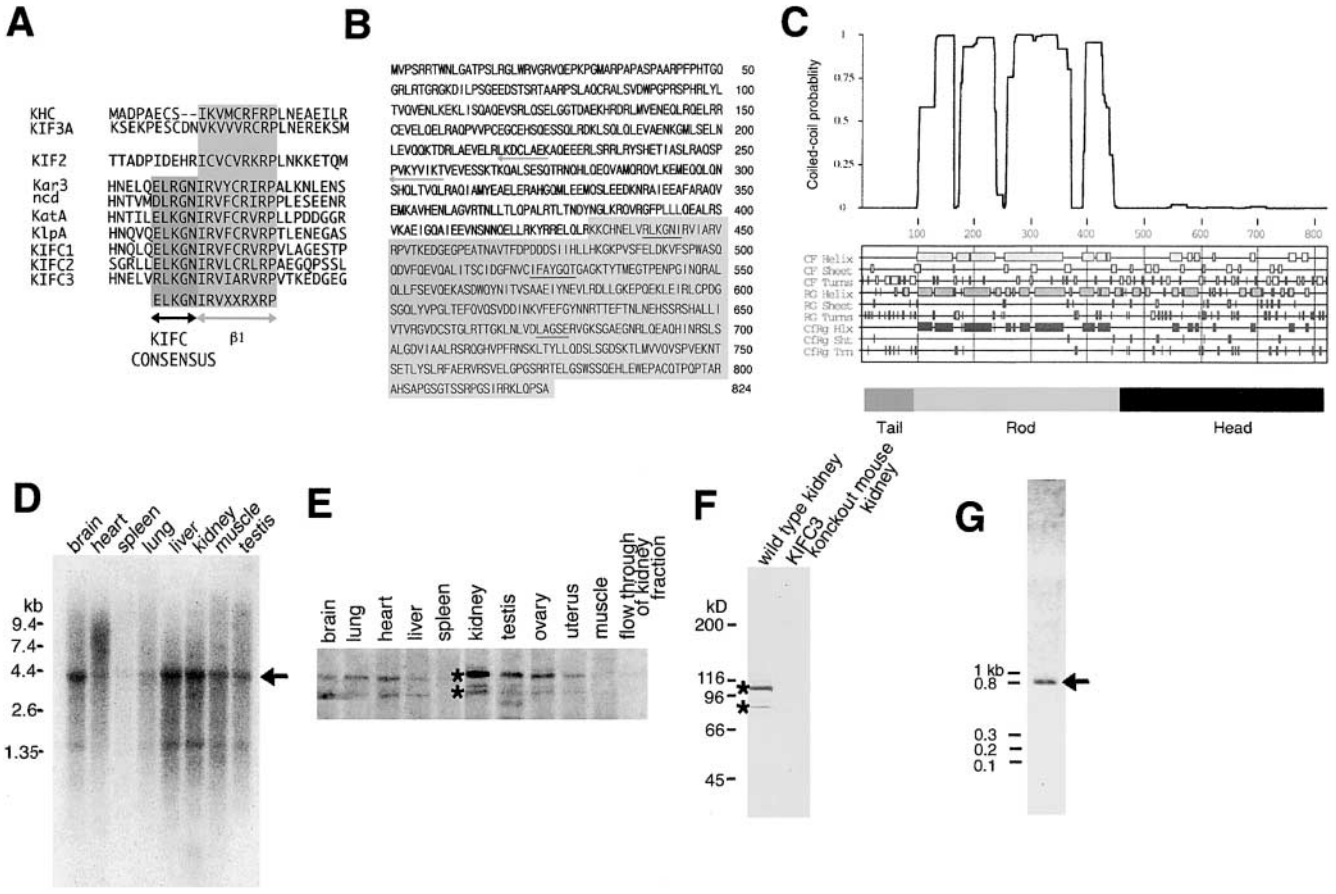

Figure 1. **Cloning of KIFC3 with KIFC consensus sequences.** (A) KIFC consensus and alignment of sequences around the β1 strand of KIFs. KIFC3 has a conserved sequence of the COOH-terminal motor domain–type KIFCs, which is not found in NH_2-terminal motor domain–type KIFs (conventional kinesin heavy chain and KIF3A) or central-type KIF (KIF2). (B) Deduced aa sequence of KIFC3. Underline shows the position of the primers used for the PCR screenings. Shading shows the region of recombinant C3S. (C) Secondary structure prediction of KIFC3. The central region of the molecule is predicted to form an α-helical coiled coil structure. (D) Northern blot analysis of KIFC3. 5 μg of mRNA from 4-wk-old ICR mouse tissues was loaded onto each lane. KIFC3 was recognized with rod domain probe as a dominant 4-kb band in the kidney, brain, and liver. (E) Tissue distribution of KIFC3 by Western blotting. Immunoprecipitation of each tissue homogenate revealed the predominant expression of KIFC3 in the kidney (asterisks), testis, and ovary. (F) Anti-KIFC3 antibody specifically recognized multiple bands in the kidney (asterisks). All of these bands were completely deleted in the kidneys of KIFC3-knockout mice. (G) Cap site hunting of the NH_2-terminal fragment of KIFC3 reverse transcription–PCR between the NH_2-terminal cap sequence and primers corresponding to sequences from 750 to 774 bp, and then from 649 to 672 bp, yielded a single band of the expected length in a mouse kidney cDNA library.

Minus end–directed motor activity of KIFC3

To estimate the in vivo function of KIF, it is important to analyze its motility characteristics (polarity, speed, and processivity), which are determined by the motor domain and its adjacent region, the so-called "neck" (Endow and Waligora, 1998; Sablin et al., 1998). Therefore, we expressed a motor domain construct of KIFC3 (C3S) that consists of an NH_2-terminal polyhistidine tag and the reactive cysteine residue, followed by a short stretch of a coiled coil stalk, the conserved KIFC consensus neck (Saito et al., 1997; Hirokawa et al., 1998b; Sablin et al., 1998), and the COOH-terminal motor domain (Fig. 1 B).

The ATPase activity of C3S was activated >100-fold in the presence of MTs with K_m (MT) values of 100 ± 30 nM. The k_{cat} of the MT-activated ATPase activity of KIFC3 was 5 ± 1 /s per head.

To determine the motor activity of KIFC3, we directly measured the movement of a single fluorescence-labeled motor protein (Vale et al., 1996; Okada and Hirokawa, 1999) on the polarity-marked MTs (Hyman and Mitchison, 1991). The degree of error of the position measurement by centroid analysis was checked by the C3S protein tightly bound to MTs in the presence of adenylyl imidodiphosphate (AMP-PNP) (Fig. 2 C), or the C3S protein adsorbed on the cover glass surface (unpublished data). The root mean square error of the position measurement was ~30 nm.

Movement of >400 molecules along MTs was observed. The mean duration of the movement was ~0.5 s (Fig. 2 A), and the movement itself was rather stochastic, mostly due to intrinsic Brownian fluctuations of the motor molecule. It should be noted that this large fluctuation is not due to the noise of the position measurement. As shown in Fig. 2 C, the variance of the displacement is much larger in the presence of ATP. Thus, this large variance reflects the intrinsic fluctuation of ATPase or motility events (Schnitzer and Block, 1997; Okada and Hirokawa, 1999, 2000). Despite this large fluctuation, they consistently moved toward the strongly labeled minus ends of MTs (Fig. 2, B and C) despite this large fluctu-

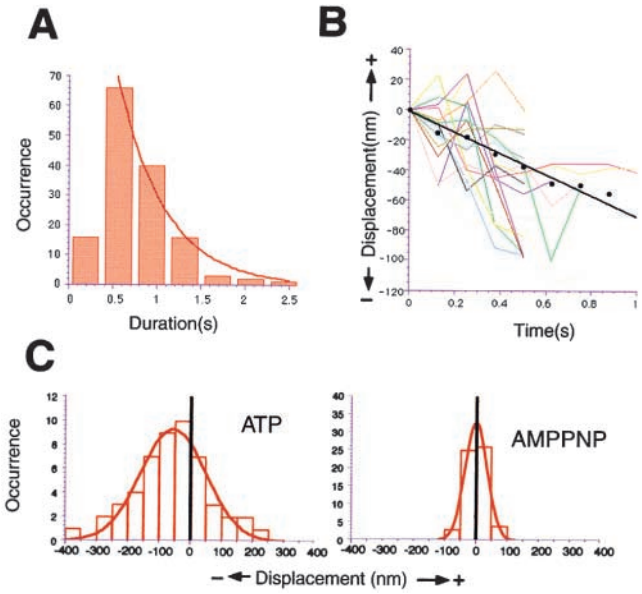

Figure 2. **Motility assay of single fluorescence-labeled recombinant KIFC3.** (A) Exponential distribution of the duration of movement, indicating that the mean duration of movement was 0.5 ± 0.1 s. (B) Plot of the displacements of individual motor spots (colored lines) and the mean displacement (black dots) against time. The first 12 motor spots on a single MT are plotted. The black line shows the average movement calculated by linear regression analysis of 50 motor spots each on eight MTs, which yielded the motor mean velocity of 75 ± 10 nm/s. To cancel the mechanical drift, only MT pairs in the same field with opposite movement direction were used for the analysis. (C) Distribution of the displacement 0.5 s after binding to MTs. Panels show the displacement in the presence of ATP (left), and of AMP-PNP (right). The left panel indicates that the distribution was biased toward the minus end of the MT in the presence of ATP, and the right panel indicates error in the position measurement because kinesin motors are tightly bound to MTs in the presence of AMP-PNP.

ation. Linear regression analysis of the entire data set (400 motor spots, 1,525 data points) revealed that, on average, the motor moved linearly toward the minus end of MT at 75 nm/s (4.5 μm/min) (Fig. 2 B, black line) ($P < 10^{-10}$), thus supporting the ATPase turnover rate ($k_{cat} = 5 \pm 1$/s per head).

Thus, the KIFC3 motor domain has an MT minus end–directed motor activity, which may be modulated or regulated by the NH_2-terminal tail region. This issue needs more investigation with full-length KIFC3 protein.

Localization of KIFC3 in renal tubular epithelial and MDCK II cells

What is the function of KIFC3 in vivo? As the first clue to the intracellular functions of KIFC3, we examined the localization of KIFC3 in the kidney. Immunocytochemical staining of renal tissues showed that KIFC3 is localized in the distal tubules (Fig. 3 Aa, D) and loops of Henle (unpublished data), but not in the proximal tubules or the glomeruli (Fig. 3 Aa, P and G, respectively), with stronger staining in the apical area of these epithelial cells (Fig. 3 Ab, arrowheads).

In polarized MDCK cells, model epithelial cells derived from canine kidney distal tubules, this apical staining pattern of KIFC3 (Fig. 3 Ba, green, arrows) was similarly observed. That is, the staining of KIFC3 was localized immediately beneath that of glycoprotein (gp) 135, a marker protein for the apical PM (Fig. 3 Ba, red) (Ojakian and Schwimmer, 1988) where apically transported vesicles accumulate. This region overlaps the area stained with annexin XIIIb, a marker protein for these vesicles (Fig. 3 Bc, green) (Lafont et al., 1998). This staining pattern suggests that the MT minus end–directed motor KIFC3 transports vesicles to the apical side where minus ends of the longitudinal MT array terminate. Immuno-EM of polarized MDCK cells confirmed that KIFC3 is apically localized on small vesicles (50–100 nm) without coatomer in a cytoplasm (apical sub-PM region) (Fig. 3 Ca, c, d, e). In this apical sub-PM region, basolateral marker protein was undetectable (unpublished data).

Association of KIFC3 with Triton-insoluble vesicles

For the biochemical characterization of these vesicular structures, we examined the behavior of KIFC3 using a flotation assay in combination with detergent extraction (Fig. 3 D). After extraction with a buffer containing 1% Triton X-100 at 4°C, the cell extract was applied at the bottom of a discontinuous sucrose density gradient (5/30%). The KIFC3-associated membrane was resistant to Triton X-100 and floated to the lighter fraction along with Fyn and annexin XIIIb, well-known components of unique Triton-insoluble, cholesterol-rich membrane subdomains (Brown and Rose, 1992; Lafont et al., 1998). The distribution of KIFC3-associated vesicles overlapped with that of KIF5B and the dynein intermediate chain (DIC), another candidate for a member of apical transport motor complex; the peak fraction of KIFC3 was lighter than that of DIC. Collectively, these data showed that KIFC3 exists in close association with the Triton-insoluble membranes (Fig. 3 D).

Specific transport of annexin XIIIb–associated vesicles by KIFC3

Both immunocytochemical and biochemical data suggest that KIFC3 is involved in the transport of apical Triton-insoluble membranes. Because the staining pattern of KIFC3 was similar to that of annexin XIIIb, a molecule apically transported from TGN to the PM (Lafont et al., 1998) (Fig. 3, Ba and Bc, green), we next examined the responses of KIFC3 and annexin XIIIb to perturbations known to affect such transport.

For the quantitative analysis of the perturbations, we adopted a quantitative immunofluorescent method. Because KIFC3 remains in the apical sub-PM region, the standard apical surface-labeling method cannot be applied. Therefore, we quantified the amount of the molecule in the apical region of the cell by measuring fluorescence intensity using quantitative confocal microscopy after immunofluorescent staining (Lippincott-Schwartz et al., 1998).

In both control and experimentally treated cells, the measured fluorescence intensities varied largely; however, their distribution was well fitted by the theoretically expected distribution, a logarithmic Gaussian distribution (Fig. 4 B) (accumulated $\chi^2 = 49.457$; $P < 10^{-128}$ by χ^2 test) (Kaplan and Meier, 1958). Therefore, in the following analyses we adopted parametric statistical tests (Student's *t* test, for example) and reported the logarithmic mean of the relative fluorescence intensity normalized by the corresponding control data sets, although nonparametric tests resulted in essentially the same conclusions.

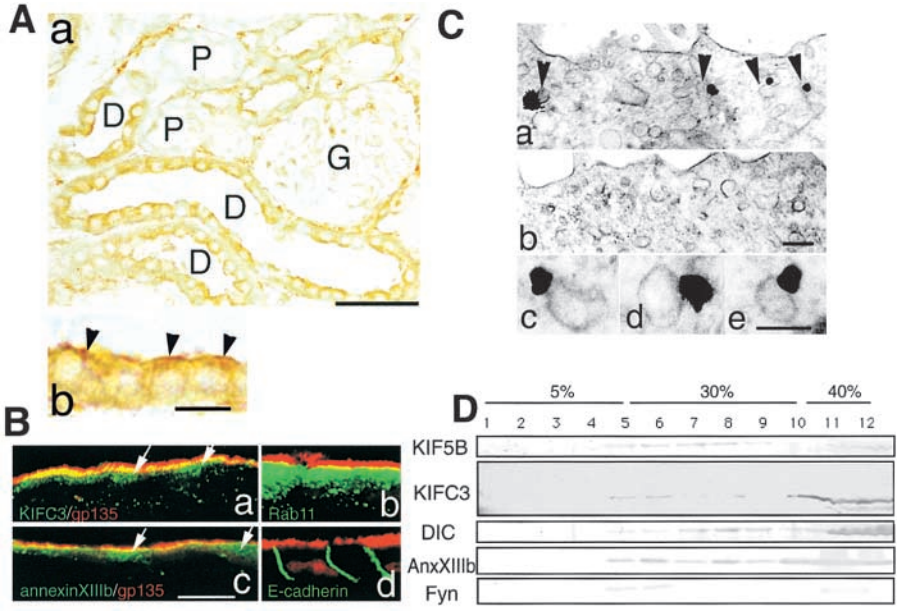

Figure 3. **Localization of KIFC3.** (A) (a) Immunohistochemistry of a section of the kidney by the ABC method. Staining of KIFC3 was preferentially localized in the distal tubules (D) as compared with that in the proximal tubules (P) or the glomeruli (G). Bar, 100 μm. (b) Higher magnification reveals accumulation of KIFC3 in the apical portion of the tubular epithelial cells (arrowheads). Bar, 20 μm. (B) Immunofluorescence staining of polarized MDCK II cells sectioned longitudinally by cryomicrotome. Green: stained with anti-KIFC3 (a), anti-rab11 (b), anti–annexin XIIIb (c), and anti–E-cadherin antibodies (d). Red: stained with anti-gp135 antibody, a marker protein of the apical PM (a–d). The nuclei were counterstained with propidium iodide (red) (Molecular Probes) in d. Dominant staining of KIFC3 in the apical portion is observed immediately beneath that of gp135 (a, arrows), which is similar to that of annexin XIIIb (c, arrowheads). Bar, 20 μm. (C) (a) Immuno-EM of polarized MDCK II cells stained with anti-KIFC3 antibody. Because the immunoreactivity of anti-KIFC3 antibody significantly decreased after 2 h of fixation, prolonged silver enhancement was performed to detect a few signals at the microscopic level, which is consistent with the immunofluorescence staining pattern. Signals are localized to small vesicles (arrows) immediately beneath the PM, but not on the PM or within microvilli. (b) Negative control. (c–e) Higher magnification. Bars: (a and b) 200 nm; (c–e) 100 nm. (D) A flotation assay, combined with 1% Triton-X extraction, reveals that part of KIFC3 floated to the lighter fractions, similar to Fyn and annexin XIIIb. KIFC3 fractions overlapped those of KIF5B (Kanai et al., 2000) and DIC, but their peak fraction is lighter than that of DIC.

First, we attempted low-temperature blocking that partially inhibits vesicular exit from the TGN (Matlin and Simons, 1983) (Fig. 4, A and B; Table I). After incubation for 90 min at 18.5°C, the apically transported KIFC3 decreased to 54 ± 2%, whereas the staining intensity of gp135 did not change (108 ± 2%) as a result of the same treatment (Fig. 4, Ab, Ab′, and B). Additional incubation at 37°C gradually restored the apical localization of KIFC3 within 30 min (96 ± 2%) (Fig. 4 Ac). This recovery was blocked by adding low concentrations of brefeldin A (BFA) (2 μg/ml) (55 ± 2%) (Fig. 4 Ad) under a combined condition known to selectively inhibit the TGN to apical surface transport without influencing ER to Golgi and clathrin-dependent endocytosis in MDCK cells (Low et al., 1992). The same treatment caused a reaction in annexin XIIIb, identical to that in KIFC3 (64 ± 1% at 18.5°C; 92 ± 2% at 37°C; and 61 ± 1% in the presence of BFA) (Fig. 4, Ae–h and B; Table I).

These quantitatively similar responses suggest that annexin XIIIb is transported by KIFC3. Therefore, we next analyzed biochemically the association of KIFC3 with annexin XIIIb–associated vesicles by immunoprecipitation and glutathione *S*-transferase (GST) pulldown experiments (Fig. 4, C and D). Annexin XIIIb–associated vesicles were purified by immunoaffinity chromatography. Anti–annexin XIIIb antibody copurified KIFC3 with annexin XIIIb from a low-speed supernatant fraction of MDCK cells; KIF5B and DIC were not detected in this fraction (Fig. 4 C). To further verify this interaction from the side of KIFC3, we expressed a GST fusion protein of a KIFC3 tail that was immobilized on glutathione Sepharose beads and incubated with the low-speed sup of MDCK cells. Annexin XIIIb was concentrated on these beads, but DIC was not (Fig. 4 D). It should be noted that annexin XIIIb is not a direct binding protein of KIFC3, because free annexin XIIIb was not concentrated on the KIFC3 tail beads (unpublished data). Collectively, these results show that KIFC3 is associated with the same vesicle as annexin XIIIb. Other MT motors such as cytoplasmic dynein and conventional kinesin (KIF5B) are absent on these vesicles.

Necessity of motor function of KIFC3 for apical transport

The next question is whether KIFC3 actively transports its associated vesicles in vivo, and if so, how does this transport contribute to the transport of the apical PM protein? To answer these questions, we first disrupted an MT network using nocodazole. After overnight incubation with 10 μg/ml nocodazole, most MTs in polarized MDCK cells were depolymerized except for a small amount remaining in the apical area (Fig. 5, Ab and Ab′, red). Such treatment significantly decreased the amount of KIFC3 in the apical sub-PM region (Fig. 5, Ab and Ab′, green) (61 ± 2% with nocodazole), indicating that intact MTs are necessary for the apical localization of KIFC3.

Next, we changed the amount of active KIFC3 protein using adenovirus vectors expressing full-length KIFC3 and a dominant–negative mutant form of KIFC3 without its COOH-terminal motor domain (aa 1–515) (headless KIFC3), and then observed the apical transport in these infected cells. The expression of each molecule was confirmed by Western blotting (unpublished data). Similar to endogenous molecules (Fig. 5 Ba–a″), full-length KIFC3 accumulated in the apical sub-PM region when overexpressed in polarized MDCK cells (Fig. 5 Bc–c″). In contrast, headless KIFC3 was distributed homogeneously throughout the cytoplasm (Fig. 5 Bb–b″). Together with the result of the MT depolymerizing experiment, these results suggest that the MT motor activity of KIFC3 is required for the apical localization of KIFC3.

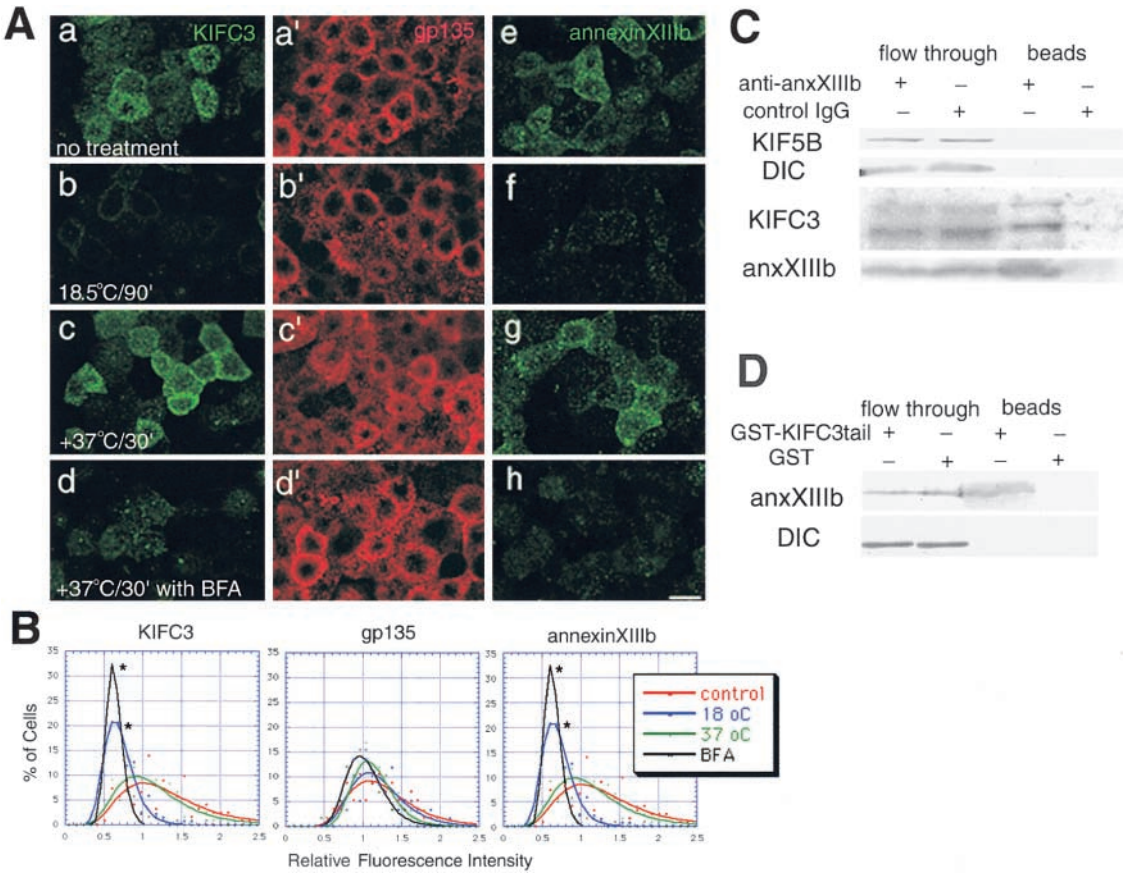

Figure 4. **Association of KIFC3 with annexin XIIIb.** (A) Localization of KIFC3 and annexin XIIIb after low-temperature blocking. Polarized MDCK cells were incubated in Dulbecco's PBS (+) buffer at 18.5°C for 90 min (b, b′, and f), followed by incubation at 37°C for 30 min (c, c′, and g). The two left columns are double stained with anti-KIFC3 (green) and anti-gp135 (red) antibodies, and the right column is stained with anti-annexin XIIIb antibody (green). (a, a′, and e) Original staining pattern before treatment. After low-temperature incubation, intensity of staining of KIFC3 (b) and annexin XIIIb (f) in the apical region decreased, which was recovered within 30 min of incubation at 37°C (c and g). BFA (2 μg/ml) inhibits this recovery even after 30 min (d and h). Bar, 20 μm. (B) Distribution of apical fluorescence intensity of KIFC3, gp135, and annexin XIIIb after low-temperature blocking and its recovery. Although fluorescence intensity of gp135 did not change with the treatment, those of KIFC3 and annexin XIIIb decreased by 46 ± 2 and 36 ± 1%, respectively. Asterisks show $P < 0.001$. (C and D) Immunoprecipitation with anti–annexin-XIIIb antibody-conjugated beads (C). KIFC3 was coimmunoprecipitated with annexin XIIIb, but DIC and the conventional kinesin (KIF5B) were not. (D) GST pulldown experiment with tail fragment of KIFC3. Similarly, annexin XIIIb was concentrated on the KIFC3-tail beads, but DIC was not.

These perturbations altered the subcellular localization of annexin XIIIb (Fig. 5, B and C; Table II). In cells overexpressing headless KIFC3, the apical accumulation of annexin XIIIb decreased to 58 ± 1% (Fig. 5, Be, Be′, and C). In contrast, in cells overexpressing full-length KIFC3, the apical accumulation of annexin XIIIb increased to 142 ± 1% (Fig. 5, Bf, Bf′, and C). In either infected cell, the total amount of annexin XIIIb was same as that in noninfected control cells (unpublished data). Thus, the observed perturbation to the localization of annexin XIIIb implies that the apical accumulation of annexin XIIIb is dependent on the motor activity of KIFC3. The fact that annexin XIIIb is the cargo membrane protein of KIFC3 suggests that KIFC3 actively transports annexin XIIIb–associated vesicles to the apical region.

Table I. **Mean relative fluorescence intensity[a] in the apical sub-PM region after low-temperature blocking**

	KIFC	gp135	annexin XIIIb
Control	100	100	100
	(n = 95)	(n = 57)	(n = 122)
18°C	54 ± 2	108 ± 2	64 ± 1
	(n = 50)	(n = 59)	(n = 135)
	$P < 10^{-17}$		$P < 10^{-26}$
37°C recovery	96 ± 2	106 ± 1	92 ± 2
	(n = 87)	(n = 58)	(n = 120)
	$P > 0.5$		$P > 0.01$
37°C recovery + BFA	55 ± 2	96 ±1	61 ± 1
	(n = 63)	(n = 58)	(n = 122)
	$P < 10^{-23}$		$P < 10^{-32}$

[a]Mean ± SEM values after normalization to those of the control experiments are reported. Number of cells analyzed is indicated in parentheses.

To further investigate the dynamics of the apically targeted membrane proteins in KIFC3-perturbed cells, we examined the transport of HA, a typical marker protein for the apical PM (Fig. 6, A and C; Table II). The HA protein was transiently expressed by the coinfection of the influenza virus and KIFC3 adenovirus. The amount of the apically transported, newly synthesized HA protein was measured quantitatively as described above. As shown in Fig. 6, A and C, reduction in KIFC3 activity by the overexpression of headless KIFC3 decreased the rate of apical accumulation of HA to 54 ± 1%,

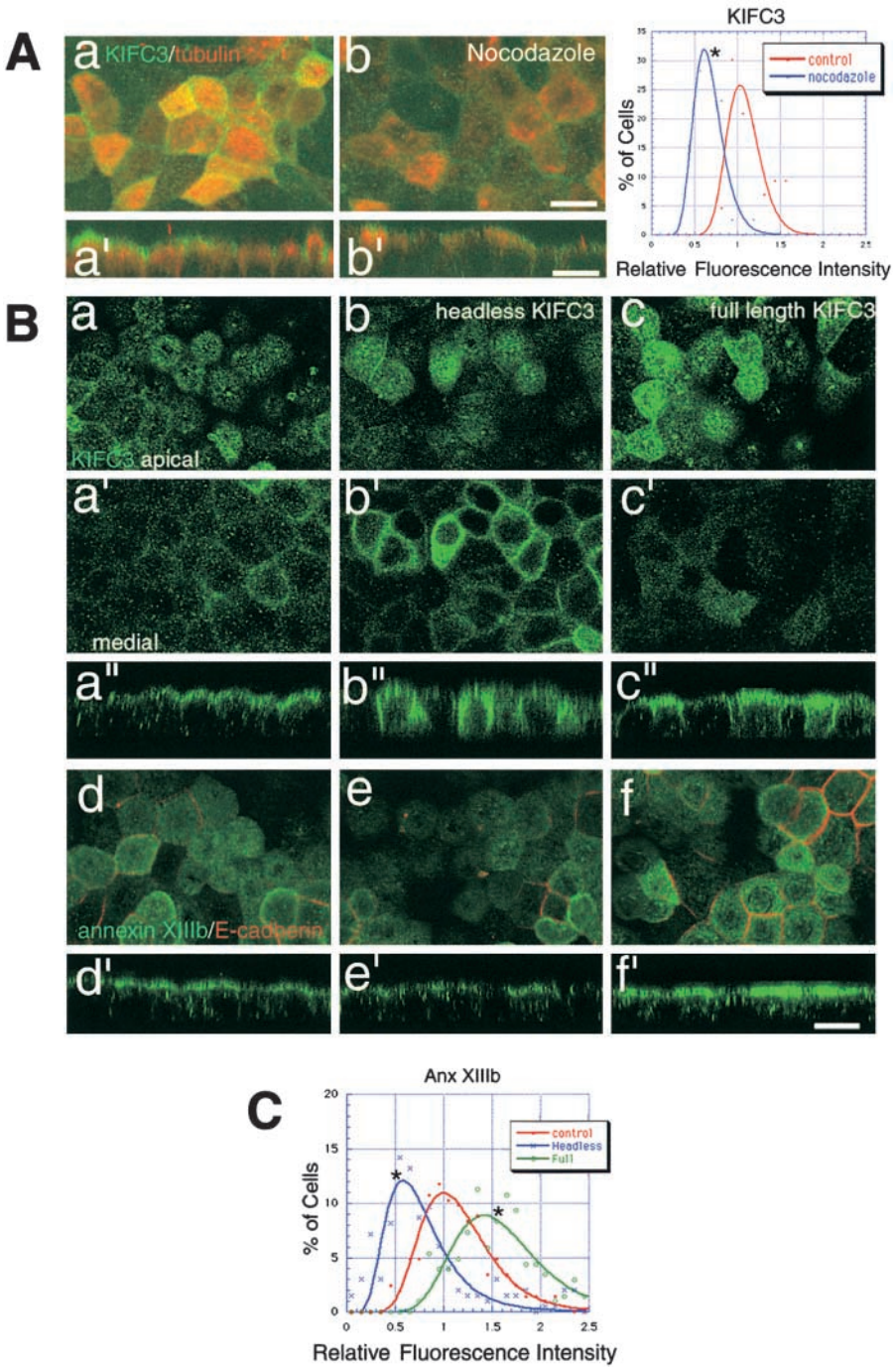

Figure 5. **Apical transport of annexin XIIIb by KIFC3.** (A) Double staining of polarized MDCK II cells using anti-KIFC3 (green) and anti–α-tubulin (red) antibodies with (b and b′) or without (a and a′) nocodazole treatment. The rate of apical accumulation of KIFC3 is reduced by depolymerizing MTs. Bar, 20 μm. (Right panel) Distribution of apical fluorescence intensity of KIFC3 after nocodazole treatment. Asterisk shows $P < 0.001$. (B) Localization of KIFC3 and annexin XIIIb in polarized MDCK II cells overexpressing recombinant KIFC3. Confocal X-Y sections in the apical (a–f) and medial (a′–c′) regions, and X-Z sections (a′′–c′′) of polarized cells stained by anti-KIFC3 antibody. Overexpressed full-length KIFC3 accumulates in the apical cytoplasm (c–c′′) similar to endogenous KIFC3 in control cells (a–a′′). In contrast, dominant–negative mutant KIFC3 (headless) evenly distributes throughout the cells (b–b′′). The rate of apical accumulation of annexin XIIIb decreased significantly in cells expressing headless KIFC3 (e and e′), compared with that in control cells (d and d′), whereas it increased in cells expressing full-length KIFC3 (f and f′). Bar, 20 μm. Apical plane of the cells is determined as the upper limit of the staining of E-cadherin localized on the lateral PM (d–f, red). (C) Distribution of relative apical fluorescence intensity of annexin XIIIb in cells expressing endogenous (red), headless (blue), and full-length exogenous (green) KIFC3s. The apical transport of annexin XIIIb was partially blocked by overexpressing headless KIFC3, whereas it was accelerated by overexpressing full-length KIFC3. Asterisks show $P < 0.001$.

whereas overexpression of active KIFC3 increased that of HA to 133 ± 1%. Because the total amount of HA protein expressed in these cells was not affected by the overexpression of KIFC3 or headless KIFC3 (Fig. 6 B), the observed change in the apical accumulation of HA reflects the efficiency of the transport of the newly synthesized, apically targeted protein to the apical sub-PM region.

This interpretation is supported by results of the immuno-EM, which directly demonstrates the colocalization of KIFC3 and HA on the same transport vesicle (Fig. 6 D, Table III). The quantitative agreement of the degrees of perturbation to the transport of annexin XIIIb and HA by the two different perturbations of KIFC3 suggests that both HA and annexin XIIIb are colocalized on the same transport vesicle (Lafont et al., 1998) whose apical transport is dependent on the motor activity of KIFC3.

Depletion of KIFC3 by acute efflux of cholesterol

Apical transport is reported to be closely related to lipid transport, particularly cholesterol transport (Keller and Simons, 1998; Heino et al., 2000). Consistently, KIFC3 is associated with a class(es) of Triton X–insoluble, cholesterol-rich vesicles (Fig. 3 D). Therefore, we examined the effect of acute cholesterol efflux from the apical PM, induced by the methyl-β-cyclodextrin (mβCD) treatment, which selectively and rapidly reduces the intracellular cholesterol content, and

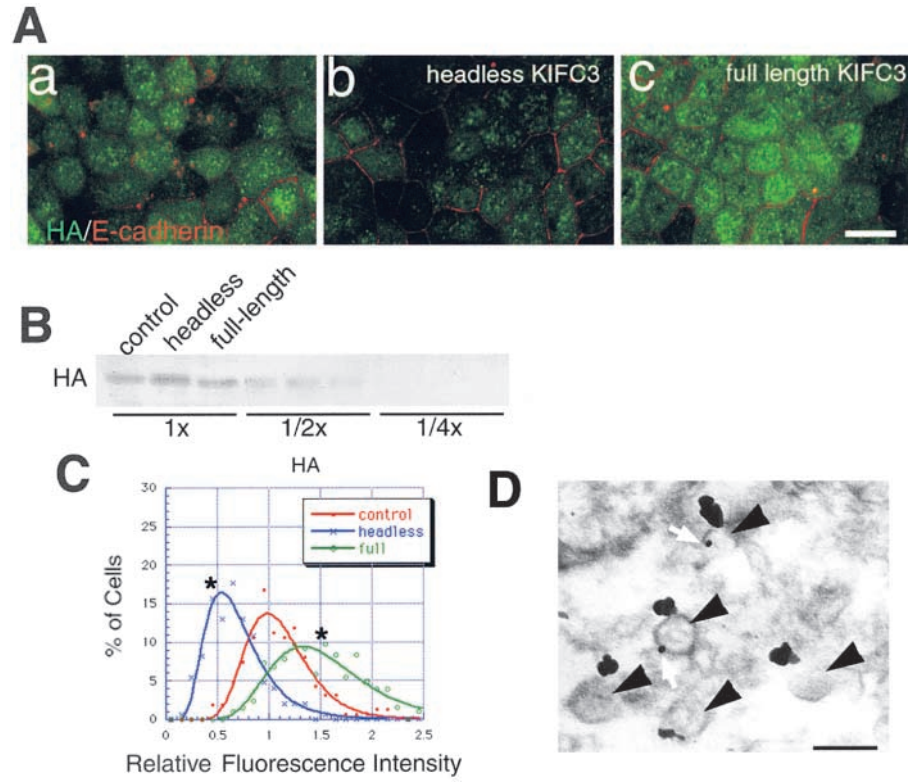

Figure 6. **Apical transport of HA by KIFC3.** (A) Apical distribution of HA (a–c, green) in cells expressing recombinant KIFC3, which are double stained with E-cadherin (a–c, red). The rate of apical accumulation of HA decreased significantly in cells expressing headless KIFC3 (b), compared with those in untreated cells (a), whereas it increased in cells expressing full-length KIFC3 (c). Bar, 20 μm. (B) Western blotting of HA in total homogenate of untreated MDCK cells, with overexpression of headless and full-length KIFC3s. The total expression level of HA was not affected by the overexpression of KIFC3, indicating that the change in the amount of HA in the apical region (A) reflects the difference in HA localization within the cells. (C) Distribution of apical fluorescence intensity of HA. HA transport was partially blocked by overexpressing headless KIFC3 (blue), whereas it was accelerated by overexpressing full-length KIFC3 (green), compared with that in the case of control (red). Asterisks show $P < 0.001$. (D) Immuno-EM of polarized MDCK cells double stained with anti-KIFC3 (0.4 nm gold; Nanoprobe) and anti-HA (10 nm gold; Amersham Pharmacia Biotech) antibodies. About one-sixth of the anti–KIFC3-labeled vesicles (arrows) were labeled with the anti-HA antibody (arrowheads). About 1% of vesicles were nonspecifically labeled in these staining conditions, but the chance of double labeling by the nonspecific staining was <0.1%. The statistical summary of this experiment is shown in Table III. Bar, 100 nm.

is expected to selectively disrupt the cholesterol-rich annexin XIIIb and HA vesicles (cargo vesicles of KIFC3) (Kilsdonk et al., 1995). Consistent with our expectation, a 60% reduction in the amount of free cholesterol in the apical PM occurred, as measured by the fluorescence intensity of combined filipin, dispersed KIFC3, and annexin XIIIb from the apical sub-PM region (Fig. 7, Ad and Ae); KIFC3 and annexin XIIIb reaccumulated rapidly after the addition of FCS for the replenishment of cholesterol. (Fig. 7, Ag and Ah). Through this process, the total amount of KIFC3 and annexin XIIIb remained constant (Fig. 7 C), indicating that the dispersion and reaccumulation of KIFC3 in the apical sub-PM region depend on the cholesterol content.

Interestingly, in contrast to the behavior of KIFC3, the fluorescence intensity of DIC in the apical region did not change with mβCD treatment (Fig. 7, Af and B), though that of DIC decreased significantly by the MT disruption with nocodazole treatment (unpublished data). This indicates that the apical localization of cytoplasmic dynein may be dependent on the MT array, but it is not associated with cholesterol-rich, apically transported vesicles like the cargo vesicles of KIFC3. This functional dis-colocalization is consistent with our biochemical and immuno-EM results: DIC was undetectable on annexin XIIIb–associated vesicles (Fig. 4, C and D), and KIFC3 and DIC showed no colocalization in immuno-EM (Table III; $P < 0.05$). Together with the results of previous studies suggesting the involvement of cytoplasmic dynein in the apical transport of HA (Lafont et al., 1994), our results suggest the existence of two independent apical transport pathways, one that is dependent on KIFC3 and one that is dependent on cytoplasmic dynein.

Table II. **Mean relative fluorescence intensity in the apical sub-PM region after overexpression of recombinant KIFC3**

	Annexin XIIIb	HA
Control	100	100
	($n = 204$)	($n = 161$)
Headless KIFC3	58 ± 1	54 ± 1
	($n = 197$)	($n = 147$)
	$P < 10^{-15}$	$P < 10^{-30}$
Full-length KIFC3	142 ± 1	133 ± 1
	($n = 204$)	($n = 205$)
	$P < 10^{-14}$	$P < 10^{-20}$

Discussion

Contribution of MT motor-dependent transport to apical membrane sorting system

To estimate the contribution of each transport process to the membrane sorting system of the polarized epithelial cells, the previously reported classical method that quantifies the final total amount of a targeted molecule at the PM is not effective; other subprocesses of the sorting system, such as selective docking and retention, may compensate for the perturbation to the transport processes. Therefore, in this report we measured the rate of apical accumulation of motor molecules and their putative cargo membrane protein in the

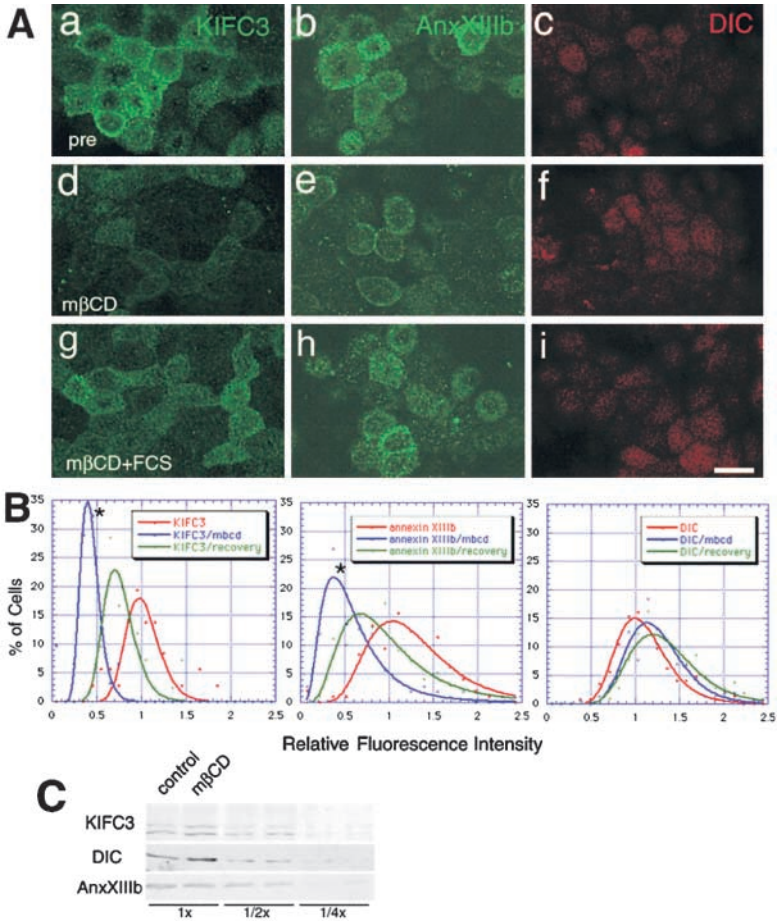

Figure 7. **Effect of cholesterol depletion on the localization of KIFC3.** (A) Dynamics of KIFC3, annexin XIIIb, and DIC after treatment with mβCD. When MDCK cells were preincubated in DME with 10 mM mβCD (Sigma-Aldrich) for 1 h before fixation (d–f), acute efflux of cholesterol in the apical PM triggered by mβCD caused the abolishment of apical staining of KIFC3 and annexin XIIIb (d and e). After a 1-h incubation in FCS-containing medium, the KIFC3 and annexin XIIIb recover in the apical region (g and h). In contrast, apical staining of DIC did not change during the same treatment (c, f, and i). Bar, 20 μm. (B) Distribution of apical fluorescence intensity of KIFC3, annexin XIIIb, and DIC after treatment with mβCD. The amount of KIFC3 and annexin XIIIb decreases after treatment with mβCD and recovers with the addition of FCS, whereas DIC shows no change. Asterisks show $P < 0.001$. (C) Western blotting of KIFC3, annexin XIIIb, and DIC in the total homogenate of MDCK cells with and without mβCD treatment. The amount of these molecules did not change by preincubation of mβCD.

sub-PM region by quantitative confocal microscopy. This new assay successfully revealed the importance of the KIFC3-, MT-, and cholesterol-dependent transport processes in the apically targeted membrane sorting system. The amount of KIFC3, as well as its putative cargo membrane proteins (annexin XIIIb and HA) in the subapical PM region, decreased proportionally as a result of the inhibition of the TGN exit with low-temperature treatment, MT disruption with nocodazole treatment, overexpression of the dominant negative mutant KIFC3 protein, and cholesterol depletion with mβCD treatment, whereas the expression of the intact KIFC3 protein increased the amount of KIFC3 and cargo proteins. Immuno-EM studies demonstrate that the subapical PM accumulation of these proteins reflects a pool of predocking transport vesicles underneath the apical PM. This accumulation suggests that docking to the PM may be a rate-limiting step of the apical sorting system. That is, apically targeted transport vesicles are rapidly transported to the subapical region where they wait for the docking and fusion processes to occur. This mechanism is analogous to regu-

Table III. **Colocalization of HA with KIFC3 and discolocalization of cytoplasmic dynein with KIFC3 on the vesicles in apical cytoplasm**

	Label			
	HA only (10 nm)[a]	KIFC3 only (0.4 nm)[a]	HA + KIFC3	No label
Observed[b]	93	49	9[c]	1198
Expected[d]	(97)	(54)	(4.4)	(1193)
	DIC only[a]	KIFC3 only	DIC 1 KIFC3	No label
Observed[b]	87	74	2[e]	734
Expected[d]	(81)	(69)	(7.5)	(740)
	Control (10 nm)	0.4 nm	Both (10 1 0.4 nm)	No label
Observed[b]	5	8	0	526
Expected[d]	(5)	(8)	(0.1)	(526)

[a]HA and KIFC3 were labeled as shown in the legend to Fig. 6 D. DIC was labeled by 10-nm gold antibody.
[b]Numbers of vesicles labeled with indicated antibodies.
[c]$P < 0.01$ by χ^2 test.
[d]Expectancy calculated on assumption of the independent distribution of the two molecules on vesicles.
[e]$P < 0.01$ by χ^2 test.

lated exocytosis, whereby tight regulation of spaciotemporal specificity is achieved through this release pool and docking machinery, as extensively analyzed in neuron synapses (Sollner and Rothman, 1994). This hypothesis can explain the discrepancy in the contribution of the MT-dependent transport step to apical membrane sorting. If the final fusion process is the rate-limiting step, the partial inhibition of the transport step will only result in the decrease in the level of the subapical pool waiting for docking, and the amount of the delivered protein on the PM surface will not be significantly affected. Therefore, to precisely understand these processes, direct and independent measurement is necessary for each transport and docking process. The use of our assay system will be the first step toward directly evaluating of the transport process.

Multiple apical transport pathway supported by different MT motors

With this new assay system, we showed that the apical transport of annexin XIIIb and HA is inhibited by a dominant–negative KIFC3, and that the transport is activated by the overexpression of intact KIFC3 (Figs. 5, B and C, and 6, A and B). These results indicate that at least some part of the apical transport system depends on the activity of the KIFC3 motor, and that the efficiency of this transport (sub)system is limited by the amount of active KIFC3 motors.

It should be noted that inhibitory perturbations to KIFC3 activity only resulted in at most a 50% decrease in the rate of apical membrane transport. This suggests that about half of the amount of apical membrane transport in stationary MDCK cells proceeds through a process independent of KIFC3, which could explain the lack of gross abnormality in KIFC3 knockout mice (Yang et al., 2001, and unpublished data).

One good candidate for the KIFC3-independent apical transport pathway is the previously proposed pathway supported by cytoplasmic dynein (Fath et al., 1997; Lafont et al., 1994). The inhibition of cytoplasmic dynein activity by the anti-dynein antibody is reported to inhibit ~70% of apically transported HA (Lafont et al., 1994). The discrepancy in the percentage of the contribution of KIFC3 and cytoplasmic dynein to the apical transport (50 vs. 70%) may not be very significant, considering that the experimental condition and the assay strategies differ significantly. Similarly, the discrepancy between the percentage of anti–KIFC3-labeled HA vesicles in our immuno-EM experiment (10%) and that of KIFC3's contribution to HA transport (50%) will not be substantial, because the efficiency of the immunogold labeling is very low. Thus, we believe that half of the amount of the apical membrane transport of stationary MDCK cells is conveyed by KIFC3, and that the other half is conveyed by cytoplasmic dynein. Consistently, cytoplasmic dynein was undetectable on immunologically purified annexin XIIIb–associated vesicles with which KIFC3 was copurified. The possibilities remain that only an undetectably small amount of cytoplasmic dynein is required for the transport, or that cytoplasmic dynein can be easily lost during the purification process. However, the differences in the subcellular distribution observed by light microscopy and immuno-EM and in response to the cholesterol perturbations, strongly support the functional differentiation of these two motors.

Although KIFC3 is ubiquitously expressed in many different tissues, its expression level differs largely among different tissues. Even in epithelial cells, KIFC3 is highly expressed in the renal distal tubule epithelium, whereas it is barely detectable in the secretory epithelium such as that of the intestine and pancreas. Interestingly, the subcellular localization of cytoplasmic dynein differs between these two classes of epithelium. In KIFC3-rich epithelial cells such as MDCK cells, cytoplasmic dynein shows a diffuse pattern in the cytoplasm by immunostaining (unpublished data), whereas it is reported to localize apically in secretory epithelial cells such as intestinal and pancreatic cells (Fath et al., 1997; Kraemer et al., 1999). This implies that ubiquitous basal apical transport by cytoplasmic dynein is supplemented by a more specific apical transport by KIFC3 in some cells. Further analysis of the molecular mechanism of cargo binding by MT motors and identification of diversified transport markers are expected to clarify the redundancy and selectivity of motor transport.

Materials and methods

PCR amplification of KIFC fragments from cDNA library and cloning of KIFC3

PCR primers were synthesized from KIFC consensus, IFAYGQT, and LAGSE sequences (Saito et al., 1997). The following processes were performed as previously described (Aizawa et al., 1992; Yamazaki et al., 1995).

Cap site hunting

Cap site cDNA and forward primers for the cap (mGppp) site region were purchased from Nippon Gene. Reverse primers were synthesized corresponding to the complementary sequences for the first and second nested PCR, which are conserved in mouse and human KIFC3 (Hoang et al., 1998).

Antibodies

Antibodies against gp135 and annexin XIIIb were gifts from Drs. G.K. Ojakian (State University of New York Health Care Center, Brooklyn, NY) and F. Lafont (European Molecular Biology Laboratory, Heidelberg, Germany). Anti-Fyn, anti-rab 11, anti-DIC, and anti-HA antibodies were obtained from Transduction Laboratory, Zymed Laboratories, Chemicon International, Inc., and Advanced ImmunoChemical, Inc., respectively.

Polyclonal antibody against recombinant KIFC3 fragments corresponding to the NH_2-terminal half of the rod domain (aa 100–250) was raised in rabbits and used after affinity purification.

Western blotting

Tissue specimens were homogenized with RIPA buffer (50 mM Tris-HCl, pH 8.0), 150 mM NaCl, 1% NP-40, 0.5% sodium deoxycholate, 1% SDS, and a protease inhibitor cocktail), centrifuged at 20,000 *g* for 10 min, and boiled. For immunoprecipitation, 1 mg of each tissue homogenate was reacted with 0.6 μg of affinity-purified anti-KIFC3. Immunoblots were detected with alkaline phosphatase–conjugated anti–rabbit IgG antibody (Cappel) or ^{125}I-labeled protein A (ICN).

ATPase and in vitro motility assays

For the ATPase and in vitro motility assays, C3S, a motor domain construct produced by PCR, was cloned into the pET21B expression vector (Novagen). Recombinant protein was expressed and purified as described (Okada and Hirokawa, 1999). MT-activated ATPase activity and single motor motility assay were performed as described previously (Okada and Hirokawa, 1999). In brief, Alexa (Molecular Probes)-labeled C3S protein was observed to move along Bodipy-labeled, polarity-marked MTs prepared according to the method of Hyman and Mitchison (1991). The resultant images were analyzed on a Macintosh computer using NIH Image software with a custom-made macroprogram for semi-automatic centroid analysis.

Cell culture

MDCK II cells were provided by Dr. E. Rodriguez-Boulan (Cornell University Medical College, New York, NY). The cells were maintained in DME (GIBCO BRL) supplemented with 5% FCS. Polarized culture was per-

formed on Transwell (Costar) as described by Bennett et al. (1988), and then harvested for 6 d.

Immunofluorescence microscopy and immuno-EM

Pre- or nonpretreated cells were fixed with a PLP fixative (4% paraformaldehyde, 10 mM $NaIO_4$, 75 mM L-lysine monohydrochloride, and 37.5 mM phosphate buffer) for 15 min, stained by the avidin biotin complex method or according to a standard immunofluorescence protocol (Noda et al., 1995), and observed under a confocal laser-scanning microscope LSM510 (ZEISS).

For immuno-EM, the sample was fixed with the PLP fixative for 2 h and processed according to the method described by Funakoshi et al. (1996).

Quantitative analysis of fluorescence intensity of immunocytochemistry

The apical plane of polarized MDCK cells was judged as upper limit of E-cadherin staining (Takara Biomedicals), or as the level of gp135. The mean density of fluorescence intensity of each cell in that plane was measured using NIH Image. Each set of data was collected from two to four independent experiments. The fluorescence intensity was normalized by the corresponding group data set, and then fitted with a logarithmic normal distribution for statistical comparison by Student's *t* test. To guarantee the robustness of this statistical analysis, nonparametric method (Wilcoxon's rank-sum test) was also performed.

Flotation assay

Polarized MDCK cells were extracted with 1% Triton X-100 containing TBS buffer (pH 8.0) for 30 min at 4°C. Crude extract was processed and applied at the bottom of the 5/30% sucrose discontinuous gradient as described by Rodgers et al. (1994).

Immunoprecipitation and GST pulldown

Recombinant KIFC3 fragments corresponding to the NH_2-terminal tail domain (aa 1–100) were expressed in *Escherichia coli* pGEX vector as GST fusion protein. They were recovered on glutathione Sepharose Fast Flow beads (Amersham Pharmacia Biotech). Polarized MDCK cells were resuspended in sucrose buffer (0.25 M sucrose, 20 mM Tris-HCl, pH 8.0, 2 mM EGTA, 1 mM DTT, 0.1% gelatin, and a protease inhibitor cocktail), homogenized by pipetting through 27-gauge needles, and centrifuged at 1,000 *g* for 20 min. The recovered supernatant was then incubated with bait-conjugated glutathione Sepharose beads or anti–annexin XIIIb antibody-fixed protein A-Sepharose 4 Fast Flow beads (Amersham Pharmacia Biotech) at 4°C overnight. The beads were washed and prepared for SDS-PAGE.

Construction of adenovirus vectors

Full-length KIFC3 and its COOH-terminally truncated form (aa 1–515) were inserted into the pAdex apCAW vector. The recombinant virus was purified and amplified according to Terada's method (1996). Polarized MDCK cells were infected from the basolateral side at 100 moi and observed after 18–24 h (Delporte et al., 1997).

We are grateful to Drs. E. Rodriguez-Boulan, F. Lafont, and G.K. Ojakian for providing us with MDCK cells and antibodies. Sincere gratitude is also extended to Dr. T.J. Mitchison (Harvard Medical School, Boston, MA) for the GMPCPP and to Dr. K. Kawasaki (National Institute of Bioscience and Human Technology, Ibaraki, Japan) for providing the influenza virus. Finally, we thank Drs. S. Kondo, S. Takeda, Y. Kanai, and other members of the Hirokawa Laboratory (Tokyo, Japan) for their technical assistance and valuable advice, and Ms. H. Sato, H. Fukuda, and M. Sugaya for their technical and secretarial assistance.

This work was supported by a special Grant-in-Aid for the Center of Excellence (N. Hirokawa) from the Japan Ministry of Education, Science, Sports, Culture and Technology.

Submitted: 8 August 2001
Revised: 29 August 2001
Accepted: 29 August 2001

References

Aizawa, H., Y. Sekine, R. Takemura, Z. Zhang, M. Nangaku, and N. Hirokawa. 1992. Kinesin family in murine central nervous system. *J. Cell Biol.* 119: 1287–1296.

Aroeti, B., and K.E. Mostov. 1994. Polarizing sorting of the polymeric immunoglobulin receptor in the exocytotic and endocytotic pathway is controlled by the same amino acids. *EMBO J.* 13:2297–2304.

Bacallao, R., C. Antony, C. Dotti, E. Karsenti, E.H. Stelzer, and K. Simons. 1989. The subcellular organization of Madin-Darby canine kidney cells during the formation of a polarized epithelium. *J. Cell Biol.* 109:2817–2832.

Bennett, M.K., A. Wandinger-Ness, and K. Simons. 1988. Release of putative exocytic transport vesicles from perforated MDCK cells. *EMBO J.* 7:4075–4085.

Bost-Usinger, L., R.J. Chen, D. Hillman, H. Park, and B. Burnside. 1997. Multiple kinesin family members expressed in teleost retina and RPE include a novel C-terminal kinesin. *Exp. Eye Res.* 64:781–794.

Breitfeld, P.P., W.C. McKinnon, and K.E. Mostov. 1990. Effect of nocodazole on vesicular traffic to the apical and basolateral surfaces of polarized MDCK cells. *J. Cell Biol.* 111:2365–2373.

Brown, D.A., and J.K. Rose. 1992. Sorting of GPI-anchored proteins to glycolipid-enriched membrane subdomains during transport to the apical cell surface. *Cell.* 68:533–544.

Calakos, N., M.K. Bennett, K.E. Peterson, and R.H. Scheller. 1994. Protein-protein interactions contributing to the specificity of intracellular vesicular trafficking. *Science.* 263:1146–1149.

Delporte, C., B.C. O'Connell, X. He, H.E. Lancaster, A.C. O'Connell, P. Agre, and B.J. Baum. 1997. Increased fluid secretion after adenoviral-mediated transfer of the aquaporin-1 cDNA to irradiated rat salivary glands. *Proc. Natl. Acad. Sci. USA.* 94:3268–3273.

Drubin, D.G., and W.J. Nelson. 1996. Origin of cell polarity. *Cell.* 84:335–344.

Endow, S.A., and K.W. Waligora. 1998. Determinants of kinesin motor polarity. *Science.* 281:1200–1202.

Fath K.R., G.M. Trimbur, and D.R. Burgess. 1997. Molecular motors and a spectrin matrix associate with Golgi membranes in vitro. *J. Cell Biol.* 139:1169–1181.

Funakoshi, T., S. Takeda, and N. Hirokawa. 1996. Active transport of photoactivated tubulin molecules in growing axons revealed by a new electron microscopic analysis. *J. Cell Biol.* 133:1347–1353.

Grindstaff, K.K., R.L. Bacallao, and W.J. Nelson. 1998. Apiconuclear organization of microtubules does not specify protein delivery from the trans-Golgi network to different membrane domains in polarized epithelial cells. *Mol. Biol. Cell.* 9:685–699.

Harder, T., and K. Simons. 1997. Caveolae, DIGs, and the dynamics of sphingolipid-cholesterol microdomains. *Curr. Opin. Cell Biol.* 9:534–542.

Heino, S., S. Lusa, P. Somerharju, C. Ehnholm, V.M. Olkkonen, and E. Ikonen. 2000. Dissecting the role of the Golgi complex and lipid rafts in biosynthetic transport of cholesterol to the cell surface. *Proc. Natl. Acad. Sci. USA.* 97: 8375–8380.

Hirokawa, N. 1998a. Kinesin and dynein superfamily proteins and the mechanism of organelle transport. *Science.* 279:519–526.

Hirokawa, N., Y. Noda, and Y. Okada. 1998b. Kinesin and dynein superfamily proteins in organelle transport and cell division. *Curr. Opin. Cell Biol.* 10: 60–73.

Hirschberg, K., C.M. Miller, J. Ellenberg, J.F. Presely, E.D. Siggia, R.D. Phair, and J. Lippincott-Schwartz. 1998. Kinetic analysis of secretory protein traffic and characterization of Golgi to plasma membrane transport intermediates in living cells. *J. Cell Biol.* 143:1485–1503.

Hoang, E.H., J.L. Whitehead, A.C. Dose, and B. Burnside. 1998. Cloning of a novel C-terminal kinesin (KIFC3) that maps to human chromosome 16q13-q21 and thus is a candidate gene for Bardet-Biedl syndrome. *Genomics.* 52: 219–222.

Hunziker, W., C. Harter, K. Matter, and I. Mellman. 1991. Basolateral sorting in MDCK cells requires a distinct cytoplasmic domain determinant. *Cell.* 66: 907–990.

Hyman, A.A., and T.J. Mitchison. 1991. Regulation of the direction of chromosome movement. *Cold Spring Harb. Symp. Quant. Biol.* 56:745–750.

Kanai, Y., Y. Okada, Y. Tanaka, A. Harada, S. Terada, and N. Hirokawa. 2000. KIF5C, a novel neuronal kinesin enriched in motor neurons. *J. Neurosci.* 20: 6374–6384.

Kaplan, E.L., and P. Meier. 1958. Non parametric estimation from incomplete observations. *J. Am. Stat. Ass.* 53:457–481.

Keller, P., and K. Simons. 1998. Cholesterol is required for surface transport of influenza virus hemagglutinin. *J. Cell Biol.* 140:1357–1367.

Kilsdonk, E.P., P.G. Yancey, G.W. Stoudt, F.W. Bangerter, W.J. Johnson, M.C. Phillips, and G.H. Rothblat. 1995. Cellular cholesterol efflux mediated by cyclodextrins. *J. Biol. Chem.* 270:17250–17256.

Kraemer, J., F. Schmitz, and D. Drenckhahn. 1999. Cytoplasmic dynein and dynactin as likely candidates for microtubule-dependent apical targeting of pancreatic zymogen granules. *Eur. J. Cell Biol.* 78:265–277.

Kreitzer, G., A. Marmostein, P. Okamoto, R. Vallee, and E. Rodrigetz-Boulan.

2000. Kinesin and dynamin are required for post Golgi transport of a plasma-membrane protein. *Nat. Cell Biol.* 2:125–127.

Lafont, F., J.K. Burkhardt, and K. Simons. 1994. Involvement of microtubule motors in basolateral and apical transport in kidney cells. *Nature*. 372:801–803.

Lafont, F., S. Lecat, P. Verkade, and K. Simons. 1998. Annexin XIIIb associates with lipid microdomains to function in apical delivery. *J. Cell Biol.* 142: 1413–1427.

Lippincott-Schwartz, J.J., J.F. Presley, K.J.M. Zaal, K. Hirschberg, C.M. Miller, and J. Ellenberg. 1998. Monitering the dynamics and mobility if membrane proteins tagged with green fluorescent protein. *In* Methods in Cell Biology. GFP Biofluorescence: Imaging Gene Expression and Protein Dynamics in Living Cells. K.F. Sullivan and S.A. Kay, editors. Academic Press, San Diego, CA. 261–281.

Low, S.H., B.L. Tang, S.H. Wong, and W. Hong. 1992. Selective inhibition of protein targeting to the apical domain of MDCK cells by Brefeldin A. *J. Cell Biol.* 118:51–62.

Matlin, K.S., and K. Simons. 1983. Reduced temperature prevents transfer of a membrane glycoprotein to the cell surface but does not prevent terminal glycosylation. *Cell.* 34:233–243.

Matter, K., and I. Mellman. 1994. Mechanism of cell polarity: sorting and transport in epithelial cells. *Curr. Opin. Cell Biol.* 6:545–554.

Mellman, I. 1996. Endocytosis and molecular sorting. *Annu. Rev. Cell Dev. Biol.* 12:575–625.

Nakagawa, T., Y. Tanaka, E. Matsuoka, S. Kondo, Y. Okada, Y. Noda, Y. Kanai, and N. Hirokawa. 1997. Identification and classification of 16 new kinesin superfamily (KIF) proteins in mouse genome. *Proc. Natl. Acad. Sci. USA.* 94:9654–9659.

Nakata, T., S. Terada, and N. Hirokawa. 1998. Visualization of the dynamics of synaptic vesicle and plasma proteins in living axons. *J. Cell Biol.* 140:659–674.

Noda, Y., R. Sato-Yoshitake, S. Kondo, M. Nangaku, and N. Hirokawa. 1995. KIF2 is a new microtubule-based anterograde motor that transports membranous organelles distinct from those carried by kinesin heavy chain or KIF3A/B. *J. Cell Biol.* 129:157–167.

Ojakian, G.K., and R. Schwimmer. 1988. The polarized distribution of an apical cell surface glycoprotein is maintained by interactions with the cytoskeleton of Madin-Darby canine kidney cells. *J. Cell Biol.* 107:2377–2387.

Okada, Y., and N. Hirokawa. 1999. A processive single-headed motor: kinesin superfamily protein KIF1A. *Science*. 283:1152–1157.

Okada, Y., and N. Hirokawa. 2000. Mechanism of the single-headed processivity: diffusional anchoring between the K-loop of kinesin and the C terminus of tubulin. *Proc. Natl. Acad. Sci. USA.* 97:640–645.

Rodgers, W., B. Crise, and J.K. Rose. 1994. Signals determining protein tyrosine kinase and glycosyl-phosphatidylinositol-anchored protein targeting to a glycolipid-enriched membrane fraction. *Mol. Cell. Biol.* 14:5384–5391.

Rothman, J.E., and G. Warren. 1994. Implications of the SNARE hypothesis for intracellular membrane topology and dynamics. *Curr. Biol.* 4:220–233.

Sablin, E.P., R.B. Case, S.C. Dai, C.L. Hart, A. Ruby, R.D. Vale, and R.J. Fletterick. 1998. Direction determination in the minus-end-directed kinesin motor Ncd. *Nature*. 395:813–816.

Saito, N., Y. Okada, Y. Noda, Y. Kinoshita, S. Kondo, and N. Hirokawa. 1997. KIFC2 is a novel neuron-specific C-terminal type kinesin superfamily motor for dendritic transport of multivesicular body-like organelles. *Neuron*. 18: 425–438.

Salas, P.J.I., D.E. Misek, D.E. Vega-Salas, D. Gundersen, M. Cereijido, and E. Rodriguez-Boulan. 1986. Microtubules and actin filaments are not critically involved in the biogenesis of epithelial cell surface polarity. *J. Cell Biol.* 102: 1853–1867.

Schnitzer, M.J., and S.M. Block. 1997. Kinesin hydrolyses one ATP per 8-nm step. *Nature*. 388:386–390.

Sollner, T., and J.E. Rothman. 1994. Neurotransmission: harnessing fusion machinery at the synapse. *Trends Neurosci.* 17:344–348.

Terada, S., T. Nakata, A.C. Peterson, and N. Hirokawa. 1996. Visualization of slow axonal transport in vivo. *Science*. 273:784–788.

Vale, R.D., T. Funatsu, D.W. Pierce, L. Romberg, Y. Harada, and T. Yanagida. 1996. Direct observation of single kinesin molecules moving along microtubules. *Nature*. 380:451–453.

Yamazaki, H., T. Nakata, Y. Okada, and N. Hirokawa. 1995. KIF3A/B: a heterodimeric kinesin superfamily protein that works as a microtubule plus end-directed motor for membrane organelle transport. *J. Cell Biol.* 130: 1387–1399.

Yang, Z. 1997. PAML: a program package for phylogenetic analysis by maximum likelihood. *Comput. Appl. Biosci.* 13:555–556.

Yang, Z., C.H. Xia, E.A. Roberts, K. Bush, S.K. Nigam, and L.B. Goldstein. 2001. Molecular cloning and functional analysis of mouse C-terminal kinesin motor kifC3. *Mol. Cell. Biol.* 21:765–770.

Yeaman, C., K.K. Grindstaff, and W.J. Nelson. 1999. New perspectives on mechanisms involved in generating epithelial cell polarity. *Physiol. Rev.* 79:73–79.